University of Bath

Sulfamerazine: Understanding the influence of slip-planes in the polymorphic phase transformation through X-ray crystallographic studies and *ab initio* lattice dynamics

*Anuradha R. Pallipurath,[‡1] Jonathan M. Skelton,[‡2] Mark R. Warren,[3] Naghmeh Kamali,[1] Patrick McArdle,[1] and Andrea Erxleben[*1]*

[1]School of Chemistry, National University of Ireland, Galway, Ireland

[2]Department of Chemistry, University of Bath, Claverton Down, Bath BA2 7AY, United Kingdom

[3] Beamline I19, Diamond Light Source, Harwell Science and Innovation Campus, Didcot, Oxfordshire OX11 0DE, England

Abstract Understanding the polymorphism exhibited by organic active-pharmaceutical ingredients (APIs), in particular the relationships between crystal structure and the thermodynamics of polymorph stability, is vital for the production of more stable drugs and better therapeutics, and for the economics of the pharmaceutical industry in general. In this paper, we report a detailed study of the structure-property relationships among the polymorphs of the model API, Sulfamerazine. Detailed experimental characterization using synchrotron radiation is complemented by computational modelling of the lattice dynamics and mechanical properties, in order to study the origin of differences in millability and to investigate the thermodynamics of the phase equilibria. Good agreement is observed between the simulated phonon spectra and mid-infrared and Raman spectra. The presence of slip planes, which are found to give rise to low-frequency lattice vibrations, explains the higher millability of Form I compared to Form II. Energy/volume curves for the three polymorphs, together with the temperature dependence of the thermodynamic free energy computed from the phonon frequencies, explains why Form II converts to Form I at high temperature, whereas Form III is a rare polymorph which is difficult to isolate. The combined experimental and theoretical approach employed here should be generally applicable to the study of other systems which exhibit polymorphism.

Introduction

Understanding polymorph transformations is extremely important, both at a fundamental and application (industrial) level. The activity, stability, processability and dissolution kinetics of a drug product depend on its solid-state structure, and so being able to rationalize and predict the most stable form of a system is critical.(1) Polymorphism is a property exhibited by a large number of organic solids, whereby a given molecule can pack into different crystal lattices depending on the kinetic and thermodynamic driving forces present at the time of crystallization. For example, different annealing temperatures can provide varying amounts of energy to enable the system to access different polymorphs.(2, 3) Kinetic products are frequently found to be metastable polymorphs, as the most stable polymorph often takes longer to form. Eventually, however, metastable polymorphs invariably convert to the most stable form, provided the two forms are enantiotropically related. This conversion, under given storage conditions, decides the shelf-life and potentially the activity of a drug. The changes in properties associated with changes in structure can also have other direct impacts on the economics of the pharmaceutical industry.

A well-known example is the case of the anti-HIV drug Ritonavir (Abbott). The active form of this drug (Form I) is metastable, and eventually converts to the more stable Form II under storage conditions. Form II is not only inactive against HIV, but also inhibits the crystallization of the active form if present in the reaction/seed mixture, which ultimately left the company with a significant financial loss.(4) Understanding the structural features which lead to particular polymorphs being favored over competing phases, and which determine physical properties and processability, is thus of paramount importance.

In this paper, we report a combined experimental and theoretical study of the polymorphism exhibited by the model drug, Sulfamerazine (SMZ). SMZ is a sulfonamide drug, used as an anti-bacterial agent in the early 20th century. While no longer in clinical use, it is still extensively used in vetenary medicine and is widely studied as a model polymorphic system,(5, 6) and for its ability to form co-crystals(7, 8) and also co-amorphous systems.(8) Indeed, a general Google Scholar search reveals that some 300 papers with Sulfamerazine in their title have been published since the 1940s, 40 of which are from the 21st century, discussing everything from clinical trials to processability and fundamental properties, while thousands more papers have been published discussing it as a part of other studies.

SMZ has three known polymorphs. The crystal structure of Form I was first reported in 1972 by Yang *et al*., with a more detailed crystallographic study by Caria *et al*. following in 1992.(5) Form II is more thermodynamically stable at room temperature, and was discovered by Acharya *et al*. in 1982.(9) A less well known third form, Form III, was discovered in 2006 by Hossain *et al*.;(6) however, since this is very difficult to isolate, it has received considerably less attention. Since their discovery, there have been extensive studies of the structure-property relationships between the three polymorphs. The main emphasis has been on the thermodynamics of the polymorph transformations and on mechanical properties such as millability, *etc*.(7, 10-22)

Zhang *et al*. reported that the thermodynamic transformation of Form II to Form I happens between 50-54 ºC,(22) while in our previous work, we discovered that Form I goes to Form II on ball milling for an hour at room temperature.(8) Milling at low temperatures leads to the amorphization of both forms.

Experimentally, it has been observed that Form I is more millable than Form II,(8) i.e. that it amorphises more easily than form II, and this was proposed to be due to the presence of slip

4

planes in the Form I structure.(8, 23) Form I owing to the presence of slip planes, was also found to have more plasticity, making it easily compressible and tabletable. (21) Sun *et al*. calculated and compared the attachment energies of different layers in various compounds and their polymorphs, with and without slip planes, using molecular-mechanics codes, and reported that, while it was possible to model polymorphs with slip planes relatively accurately, they were not able to extend the procedure to the more stable polymorphs of the compounds.(23) Beyond this, and "conventional wisdom" from inspecting crystal structures, however, there has been little work done thus far to investigate the fundamental relationship between slip planes and millability.

For understanding both the mechanical properties of a system, and also the thermodynamics of the phase equilibria between polymorphs, *ab initio* lattice-dynamics calculations, carried out e.g. within the density-functional theory (DFT) framework, may be informative. Whereas standard total-energy calculations can provide only differences in the athermal (i.e. 0 K) lattice energies between polymorphs, lattice-dynamics calculations provide access to thermodynamic free energies as a function of temperature, based on the thermal population of the vibrational modes of the system. These calculations allow the temperature dependence of a number of properties to be evaluated from first principles, for example the constant-volume (Helmholtz) or constant-pressure (Gibbs) free energy, the thermal expansion, and the bulk modulus.(24) Given the often subtle energy differences involved in polymorphism (typically on the order of a few kJ mol^{-1}), differences in zero-point vibrational energy and/or temperature-dependent vibrational internal energy and entropy may be sufficient to overcome differences in lattice energy, and hence to shift the free-energy ordering of competing phases. In addition, knowledge of the vibrational modes of a structure, in particular of the low-frequency collective motions which are thermally

accessible at low-to-moderate temperatures, may provide insight into which internal motions within the unit cell are particularly low in energy, and hence how the structure may preferentially deform under *e.g.* mechanical shear.

In this study, we have carried out a combined experimental and theoretical characterization of SMZ, using *ab initio* lattice-dynamics calculations in conjunction with modelling of the mechanical properties, to address several important questions about this system: 1) why is Form I more millable than Form II, and 2), how is this related to the presence of slip planes?; 3) Why does Form II convert to Form I only on heating?; and 4) why is Form III so difficult to isolate? We evaluate critically the utility of DFT lattice-dynamics calculations in reproducing experimental data, demonstrating good reproduction of the atomic thermal motion and vibrational spectra of SMZ polymorphs, and illustrate how this approach can be used to obtain new insight into polymorphism in molecular crystals.

Experimental methods

Sulfamerazine (SMZ) was purchased from Sigma-Aldrich and used as received. All solvents were used as received, without further purification. SMZ Form I **(CCDC code: SLFNMA02)** was prepared by sublimation *in vacuo* at 423 K (160 ºC, <200 mbar). Form II **(CCDC code: SLFNMA01)** was prepared according to the procedure in Ref. (5), by preparing seeds by ball milling Form I for 60 minutes, which were then used to seed a solution of SMZ in an 80:20 mixture of acetonitrile and water once cooled to room temperature after initial heating. We were unable to isolate SMZ Form III **(CCDC code: SLFNMA03)** from dimethylformamide according to the reported method,(6) which in our experiments invariably resulted in the crystallization of solvates rather than the pure compound.

Variable-temperature single-crystal studies were carried out using an in-house Agilent Xcalibur S diffractometer. A full hemisphere of data was acquired in each experiment, using Mo-Kα radiation (λ = 0.71069 Å) with a graphite monochromator. The structures were solved using the SHELXT(25) software, and refined using SHELXL,(26) with all non-hydrogen atoms being refined anisotropically. ORTEX plots were generated using the OSCAIL software.(27)

A more comprehensive set of measurements were performed at the Diamond Light Source, Beamline I19, to obtain structures with a finer temperature resolution. Full crystallographic datasets were collected between 150 K and 300 K in steps of 10 K using the Crystal Logic goniometer with a Rigaku Saturn 724+ detector at beamline I19 of the Diamond Light Source synchrotron (U21 undulator, λ = 0.6889 Å, ω-scan, 1.0°/frame). The temperature was controlled using a Cryostream 700 Plus (Oxford Cryosystems) open-flow nitrogen-cooling device with a ramp rate of 120 K/hour between temperature measurements. Crystals were selected and mounted without cutting or manipulation, which we found led to peak splitting in the diffraction patterns. The data was processed in CrysAlisPro 171.37.35 using the dtrek input module, and solved using the methods described above.

Combined differential-scanning calorimetry (DSC) and thermogravimetric analysis (TGA) measurements were carried out using a Rheometric Scientific STA 625 (calibrated using an Indium standard) between room temperature and 523.15 K (250 ºC), with a heating rate of 5 K/min, to study the transformations between Form I and II (see Figure S1 for the DSC traces).

Raman and mid-infrared (MIR) spectra of both forms were acquired using a Witec Raman system (785nm laser excitation, <500 mW laser power, 64-scan integration with 0.5 s accumulation time, 4 cm^{-1} resolution within a 100-1800 cm^{-1} spectral range) and a Perkin Elmer

SpectrumOne (Waltham, Massachusetts; 400-3400 cm^{-1} range, 4 cm^{-1} resolution, 32-scan integration), respectively.

Lattice-dynamics calculations

Lattice-dynamics calculations refer generally to modelling the phonon modes of a periodic system. A good overview of the theoretical framework may be found in Dove (1993),(28) and is briefly summarized in the following.

The standard model is to treat a crystal of N atoms as $3N$ independent quantum-harmonic oscillators, which is generally sufficient to describe vibrational properties quantitatively up to moderate temperatures.

The key computation is the evaluation of the interatomic force-constant (IFC) matrices, which capture the change in force on an atom j in response to the displacement of an atom i by a small distance from its equilibrium position (eq. 1):

$$\Phi_{\alpha\beta}(il, jl') = -\frac{\partial F_\alpha(il)}{\partial r_\beta(jl')} \tag{1}$$

The subscripts α and β are the Cartesian directions x, y and z, and the indices l and l' denote the unit cells in which atoms i and j reside relative to one another. In periodic systems, phonons are modelled in reciprocal space, with an associated wavevector **q** which describes the propagation and modulation of the atomic-displacement wave across unit cells. The range of the IFCs (values of l and l') which needs to be considered to accurately model the variation (dispersion) of phonon frequencies with **q**-vector depends on the number of atoms in the unit cell, with long-range IFCs being most important for treating short-wavelength vibrations.

The force-constant matrices can be obtained either by the "direct" (finite-displacement) method, where symmetry-inequivalent atomic displacements are physically performed and the resulting forces computed, or by a perturbation-theory approach such as density-functional

perturbation theory (DFPT). The latter method can be easily extended to obtain long-range IFCs, whereas to do this in a finite-displacement approach requires performing calculations on a supercell of the initial structure.(29)

In principle, the DFPT approach is more accurate, as the calculated force constants do not depend on a displacement-step size; in the finite-displacement method, the step must be chosen carefully so that displacements do not go beyond the harmonic region of the bond-stretch potential, but do produce changes in force which are measurable above the numerical noise in the calculations. However, DFPT phonon calculations are not a standard feature of periodic DFT codes, and, even where these calculations are implemented they are often not possible with all functionals, and can also be computationally less convenient than the finite-displacement method. For these reasons, we adopted the finite-displacement approach in the present study.

The force constants are then used to build up 3×3 blocks of the dynamical matrix for a given **q**-vector, diagonalization of which produces eigenvectors and eigenvalues corresponding to the normal-mode coordinates and associated oscillator frequencies, respectively (eq. 2):

$$D_{\alpha\beta}(i,j,\mathbf{q}) = \frac{1}{\sqrt{m_i m_j}} \sum_{l'} \Phi_{\alpha\beta}(i0,jl')\exp\left[i\mathbf{q}.\left(\boldsymbol{r}(jl') - \boldsymbol{r}(i0)\right)\right] \qquad (2)$$

where m_i is the mass of atom i, and $\boldsymbol{r}(il)$ is the position of atom i in the lth unit cell. It is worth noting that a dynamical matrix for a given **q**-vector can be constructed from IFCs computed to an arbitrary range, allowing phonon frequencies to be obtained with a fine Brillouin-zone sampling without requiring explicit calculation of the IFCs in all the unit cells involved in the modulation period.

Harmonic lattice-dynamics calculations also enable the calculation of the constant-volume (Helmholtz) thermodynamic free energy, A, as a function of temperature, which for a periodic system is given by:

$$A(T) = U_L + U_V(T) - TS_V(T) \qquad (3)$$

where U_L and U_V are the lattice and vibrational internal energies, respectively, and S_V is the vibrational entropy. We note that the Helmholtz energy is the constant-volume analogue of the more familiar Gibbs free energy.

With knowledge of the phonon frequencies, it is convenient to compute the Helmholtz energy from the partition function, Z, given by:

$$Z(T) = \exp\left(-U_L/k_BT\right) \prod_{\mathbf{q}v} \frac{\exp\left(-\hbar\omega(\mathbf{q}v)/2k_BT\right)}{1 - \exp\left(-\hbar\omega(\mathbf{q}v)/2k_BT\right)} \qquad (4)$$

where ω are the phonon frequencies of the v modes at each wavevector $\mathbf{q}$, and the product captures the statistical occupation of phonon energy levels at a given temperature according to the Bose-Einstein distribution. The Helmholtz energy can then be obtained from the bridge relation:

$$A(T) = -k_B T \ln Z$$

$$= U_L + \frac{1}{2} \sum_{qv} \hbar\omega(\mathbf{q}v)$$

$$+ k_B T \sum_{qv} \ln\left[1 - \exp\left(-\hbar\omega(\mathbf{q}v)/2k_B T\right)\right] \tag{5}$$

The right-hand side of Eq. 5 shows that the Helmholtz energy is a sum of three terms, *viz.* the lattice energy, a sum of the zero-point vibrational energies of each mode, and a temperature-dependent term arising from the population of phonon energy levels, which contains part of U_V plus the entropic contribution to the free energy. It is worth noting that U_L is the only component of the free energy which is available from standard total-energy calculations, and, in this model, the temperature dependence of the free energy is thus only available from the lattice dynamics.

In addition to $A(T)$, it is also possible to evaluate the temperature dependence of the internal energy and entropic contributions separately. The former can be evaluated directly according to:

$$U(T) = U_L + U_V(T) = U_L + \sum_{qv} \hbar\omega(\mathbf{q}v)\left[\frac{1}{2} + \frac{1}{\exp(\hbar\omega(\mathbf{q}v)/k_B T) - 1}\right] \tag{6}$$

where again the phonon occupation numbers are obtained from a Bose-Einstein distribution using the vibrational frequencies. The entropy can be obtained from the standard thermodynamic relation $S = \partial A/\partial T$.

Computational methods

Computational modelling was carried out on the CCDC structures of Forms I, II and III (see Experimental section for codes) within the density-functional theory (DFT) framework as implemented in Quantum ESPRESSO code.(30) The internal coordinates were optimized using three different DFT functionals, namely the Perdew-Burke-Enzerhof (PBE)(31) functional, the variant of PBE revised for solids (PBEsol),(32, 33) and the dispersion-corrected PBE-D2 functional.(34) All calculations were carried out using projector augmented-wave (PAW) pseudopotentials(35) with a plane-wave kinetic-energy cut-off of 70 Ry. The Brillouin zones of the Form I and III structures were sampled using Monkhorst-Pack k-point meshes(36) with $1\times1\times3$ and $1\times3\times1$ subdivisions, respectively, while the Form II electronic structure was modelled at the Γ point. We found from convergence testing that these parameters were sufficient to converge the absolute total energies to within 1 meV atom^{-1}. A tolerance of 10^{-6} Ry was enforced during electronic minimizations, and structural optimizations were performed to tolerances of 10^{-4} Ry and 10^{-3} Ry bohr^{-1} on the total energy and forces, respectively.

Ab inito lattice-dynamics calculations were performed using the Phonopy package,(37) using a custom-made wrapper around its Vienna *ab initio* Simulation Package (VASP) interface to convert to and from the Quantum ESPRESSO file formats. Harmonic-phonon calculations were carried out using the finite-displacement method with a step size of 0.01 Å. A tolerance of 10^{-3} Å on the atomic positions was applied during the detection of the space group, and the calculated force constants were symmetrized appropriately. We neglected the possibility of long-range interactions between unit cells, and thus carried out the phonon calculations on single unit cells for all three systems. However, when constructing the phonon density of states and performing thermodynamic integration during post-processing, the Brillouin zone was sampled with a **q**-

point mesh with 32×32×32 subdivisions; whereas this led to little perceptible change to the phonon DOS compared to evaluating only the Γ-point frequencies, we found that the larger mesh was necessary to converge the thermodynamic free energy.

To study the mechanical properties of the three polymorphs further, we also computed energy/volume curves for each structure with PBE-D2. To do this, the cell shape and internal positions were optimized for a range of fixed volumes about those from the reported crystal structures, to the same tolerances used for the position optimization. The *E/V* data was then fitted to the Murnaghan equation of state(38) to obtain the equilibrium volume, density and bulk moduli of the three polymorphs.

The present version of Quantum ESPRESSO does not contain the necessary infrastructure for calculating elastic tensors, from which other properties (e.g. the shear moduli) can be derived. Therefore, we performed further calculations using VASP,(39) which implements the method described in Ref (40). These calculations were carried out with the PBE-D2 functional and similar technical parameters to the other calculations, *viz*. comparable PAW pseudopotentials,(41) a plane-wave cutoff of 800 eV, and the same *k*-point sampling. The elastic-constant calculations were performed on models at the equilibrium volumes obtained from the *E/V*-curve fitting (see results) after optimisation of the internal ion positions and cell shape. These optimizations were carried out to a force tolerance of 10^{-2} eV Å^{-1}, and tolerences of 10^{-6} and 10^{-8} eV for the electronic minimization were enforced during the geometry optimization and elastic-constant calculations, respectively.

Results and discussion

Variable-temperature crystallography

The literature structures of the three forms of SMZ are shown in Figure 1. Form I crystallises in the $Pna2_1$ space group with two molecules in the asymmetric unit and eight molecules in the unit cell, which form a layered structure along the crystallographic c axis.(5) Form II crystallises in a $Pbca$ structure with one molecule in the asymmetric unit and eight in the unit cell.(5) In contrast, Form III has one molecule in the asymmetric unit and four in the unit cell, and adopts the $P2_1/c$ space group.(6) The unit-cell parameters of the three structures are given in Table 1 for comparison. The three different polymorphs have distinctly different H-bonding patterns, and Forms I and III contain slip planes, which lie perpendicular to the b axis and parallel to the b and c axes, respectively.

To provide an experimental reference for the computational modelling, and in particular to obtain insight into the thermally-accessible lattice motions from an analysis of the thermal ellipsoids, we performed variable-temperature single-crystal X-ray diffraction experiments using both an in-house instrument and synchrotron radiation. Figure 2 shows the density of Forms I and II as a function of temperature, and the corresponding percentage changes in the lattice parameters. Due to the difficulty we had in obtaining Form III, we were not able to carry out similar experiments on this polymorph.

The difference in the nature of the bonding in the two polymorphs is well reflected in the anisotropic expansion observed along the three crystallographic axes in both unit cells. In Form I, the crystallographic c-axis undergoes significantly larger expansion than the a and b axes. From the in-house data, the a axis appears to stop expanding beyond 200 K, whereas in the higher-resolution synchrotron data the expansion is roughly linear from 150-300 K but with a

shallow gradient. In the case of Form II, maximum expansion is observed along the b axis, which corresponds to the stacking direction of the herringbone "layers". Conversely, minimum expansion occurs along the c direction, which would require stretching the intermolecular H bonds. The percentage expansion of the Form II lattice is on the same order as that of Form I, but the latter maintains a lower density throughout the temperature range studied.

Interestingly, while Form I undergoes predictable thermal expansion, indicated by the near-linear decrease in density with temperature, there is a visible break in the thermal expansion of Form II between 150 K and 185 K in the in-house data. This prominent feature is spread across a smaller temperature range and is less evident in the synchrotron data, however, suggesting that it may be crystal dependent, but some small anomalies are still apparent, in particular a subtle change in gradient of the expansion of the b axis around this temperature region. These observations could be indicative of a phase transition, although we observed no clear change in the structure over that temperature range, and the crystal remained in the same space group throughout.

Aside from this discrepancy, the synchrotron study gave a general trend in good agreement with our in-house collections. It is perhaps noteworthy that the differences in the densities amount to fairly small variations in the lattice parameters (see Tables S1-S8), and so the differences in thermal expansion may as noted be simply due to differences between the crystals used in the various data collections. Another potential factor is that data collections could be performed in 30 minutes per temperature at the synchrotron source, whereas the equivalent experiment took eight hours per temperature on the in-house instrument, allowing the structure to equilibrate for much longer at a given temperature.

A lot of information about the crystal dynamics can be gleaned from studying the displacement parameters (DPs) arising from the thermal fluctuations at different temperatures (Figure 3). In both polymorphs, there is significant inherent molecular flexibility evident even at 150 K. The carbon atoms on the benzene rings bearing the methyl groups have relatively large thermal ellipsoids compared to the rings bearing the amino groups. With increasing temperature, the size of the DPs on all the atoms increases, but, interestingly, the motion of the ring bearing the methyl group, and also that of the methyl C itself, is anisotropic, suggestive of a "rocking" motion of the ring about the S-C and S-N bonds. There is likewise a considerable increase in the DPs on the atoms in the amino ring with temperature, and these are again anisotropic, suggesting a similar behavior.

Form II, in comparison to Form I, appears to have much less flexibility, in particular in the motion of the ring bearing the amino group, with the ellipsoids on that pendant group being more isotropic than those of the atoms on the methyl ring. This is consistent with the interlayer spacing in Form I, i.e. the distance between molecules either side of the slip plane, providing more freedom for the rings to move. An overlay of the structures determined across the temperature range we studied (Figure S2) revealed little change for Form II, while Form I displayed a considerably more significant increase in the degree of molecular motion.

Molecular motion in crystals has been studied in the past using NMR, where the inherent atomic motion and the phase transition in the crystalline form of chloroform were characterized by studying the relaxation times as a function of inverse temperature.(42) More recently, the thermal motion of organic-molecular crystals has also been studied using lattice-dynamics calculations to predict anisotropic-displacement parameters (ADPs) due to thermal motion at low temperature, giving generally good correspondence with low-temperature neutron-scattering

data.(43) In the present work, from our *ab initio* lattice-dynamics calculations we were similarly able to identify numerous soft phonon modes corresponding to the motion of the two rings and their pendant functional groups, which explains the anisotropy observed in the DPs; this will be discussed further in the following subsections.

Ab-initio lattice-dynamics calculations

We first performed a set of harmonic-phonon calculations on the optimized initial structures with our three chosen functionals.

PBE and PBEsol are both based on the generalized-gradient approximation (GGA) for electron exchange and correlation. This model suffers from a fundamental limitation whereby GGA functionals must be constructed with a bias towards describing energetics (e.g. total and atomization energies) or structural properties (e.g. lattice parameters, phonon frequencies, *etc*.) accurately, but cannot do both simultaneously.(32) This is the origin of the well-known "under-binding" phenomenon commonly exhibited by PBE,(44-47) which is optimized for the former, whereas PBEsol has been shown to reproduce structures and lattice dynamics with very good accuracy.(24) The DFT-D2 method(34) adds a semi-empirical dispersion correction to the energies and forces predicted by the underlying functional (here PBE), which can improve performance in systems where dispersion (van der Waals) forces are prominent.

The three sets of initial phonon DOS curves are compared to the experimentally-recorded MIR and Raman spectra in Figures S4-S6, and a general assignment of modes can be found in Refs. (8, 48). We found that the best agreement between the positions of the peaks in the calculated phonon DOS curves and the measured spectra of Form I and II was obtained with the PBE-D2 functional. The match was especially good in the low-wavenumber and fingerprint regions of the

spectrum. A more noticeable offset between the calculated and measured peaks was observed in the high-frequency stretch region of the spectrum between 2500 and 3600 cm^{-1}; we found that this region was better reproduced by PBEsol, but that this functional gave a less good reproduction of the spectrum as a whole. When compared to both these functionals, we found that PBE yielded a phonon spectrum which was notably red shifted with respect to those obtained from the other two functionals, and also compared to the experimental measurements. Since the low-frequency phonons provide the main contribution to the vibrational free energy at finite temperature, we expect PBE-D2 to be the most suitable of the three for the present calculations.

We observed imaginary (negative-frequency) modes in all three of the phonon DOS curves, which are an indicator of structural instability. These modes invariably corresponded to the inherent motion of the crystal visible in the DPs (see Figure 3), which suggests that the room-temperature structures reported in Refs. (5, 6, 9) are crystallographic averages over soft phonon modes. To attempt to get to the "true" equilibrium structure, within the constraints of the experimental unit cell, we generated structures with the atoms displaced along the imaginary-mode phonon coordinates, then re-optimized the internal positions. This mode-following procedure invariably led to a loss of the symmetry of the cell, as a result of which performing additional phonon calculations on these structures required single-point calculations on a considerably larger number of displaced structures. We therefore performed a second set of phonon calculations with only the PBE-D2 functional.

The all-electron PAW lattice energies of the three polymorphs, obtained with the three functionals before and after following the imaginary modes, are collected in Table 2. For comparison, the calculated zero-point energies obtained from the various phonon calculations are

shown in Table 3, while Figure 4 compares the final PBE-D2 phonon DOS curves against the MIR and Raman spectra collected from Form I and Form II samples.

Based on the work in Ref. (22), we would expect that Form II, as the most thermodynamically-stable form of SMZ, should have a lower combined lattice and zero-point energy than Form I. For the lattice energies, this was the case in the PBEsol and PBE-D2 calculations, which predicted Form II to be 0.49 and 6.40 kJ mol^{-1} per molecule more stable than Form I, respectively. In contrast, however, PBE predicts Form I to be the more stable of the two, by 2.62 kJ mol^{-1} per molecule. This is perhaps surprising given that PBE is in principle optimized to reproduce energetics; this could be due to our fixing the lattice parameters to the experimental values, and hence the structures not being at the PBE energy minimum. All three functionals predict Form III to have a higher lattice energy and thus to be less stable than both of the other two polymorphs, which provides an explanation as to why it is the most difficult of the three to isolate. Mode following changed some of the energy differences by up to approx. 10 %, but did not change the stability ordering.

Interestingly, the differences in the calculated zero-point vibrational energies (ZPEs) are on the same order as the difference in lattice energies, highlighting the potential importance of considering the free energy when assessing polymorph stability. Before mode following, all three functionals predict Forms II and III to have a higher ZPE than Form I. For PBE-D2, the ZPE contribution to the free energy at 0 K does not change the relative stability of the polymorphs, although it does reduce the energy difference between Forms I and II by around 30 %. For PBE, on the other hand, the zero-point energy contributions lead to Form III being more stable than Form II at 0 K, while for PBEsol the differences in ZPE are sufficient to raise Form II above

Form I in energy. As for the lattice energies, mode following changed the ZPEs obtained with PBE-D2 slightly, but this did not alter the stability ordering of the systems.

To investigate the variation in relative stability with temperature, we compared the Helmholtz free energies and vibrational internal energy and entropy as a function of temperature from 0 to 600 K (Figure 5). The free energies of Forms I and II cross around 281 K, which is remarkably close to the 320-330 K phase-transition temperature observed experimentally.(22) Even though the difference is large in temperature terms, it corresponds to a few meV in energy units, which is close to the limit of accuracy in the DFT calculations; this point is returned to in the Discussion section. Despite the potential limitations involved, however, the phase transition temperature is predicted with reasonable accuracy, and the trend is consistent with experiment.

From Figure 5c, it can be seen that the crossover comes about from a significant difference in the vibrational entropy (S_V) of Form I, which at higher temperatures is sufficient to offset the lower lattice energy of Form II. The increased entropy is attributable to soft lattice vibrations, such as are reflected in the thermal ellipsoids, the population of which can increase the entropy of the system without incurring a large internal-energy penalty. From this analysis, the high-temperature stability of Form I may be related to the presence of the slip plane and consequent reduced density, which allow for lower-energy molecular motions.

We note that an experimental study similar to recent work by Chang *et al.*,(49, 50) who used ultra-low frequency Raman spectroscopy to study temperature-dependent polymorphic transformations and performed Raman imaging to observe the growth of a second polymorph at the edges of a crystal of 1,1'binaphtyl, might be used to further investigate the results from these calculations.

Interestingly, these calculations predict that Form III remains unstable with respect to the other polymorphs even at high temperature. Although it is has a larger entropy than Form II at higher temperatures - which, as for Form I, is most likely due to its layered structure - it remains above Form I in energy up to at least 600 K (i.e. above the Form I melting temperature). Furthermore, this entropic stabilization is insufficient to offset the differences in lattice and vibrational internal energy with respect to Form II. If it is indeed the case that Form III is thermodynamically unstable with respect to Forms I and II, these calculations provide a natural explanation for why it is only possible to isolate it under very specific conditions.

Lattice dynamics and slip planes

As noted earlier, Form I of SMZ is more millable than Form II, making the former easier to process,(23) due to the presence of slip planes. However, aside from the computational modelling by Sun *et al*. to probe this indirectly *via* calculation of attachment energies,(23) which gave good results for polymorphs with slip planes, but was less successful for those without (e.g. herringbone structures), little work has been done to link this structural feature to millability. Figure 6 (a) shows the indexed faces of a single crystal of SMZ Form I, with the *c*-axis normal to the hexagonal sheet-like [001] plane. When pressure is applied to the crystal normal to the *c* axis, the layers readily slip, as can be seen in the photograph in Figure 6 (b).

From an analysis of the phonon eigenvectors obtained from the lattice-dynamics calculations, a large number of low-frequency modes related to the "rocking" of the benzene rings in the SMZ molecule about the S-C bond are clearly observed. This explains the origin of the size and, where applicable, the anisotropy of the thermal ellipsoids in the ORTEX plots noted in the previous

section (see also Figure 3). Animations of examples of these modes are supplied along with the supporting information.

For Forms I and III, which have layered structures, these motions would aid in the separation of the layers, and hence reinforce the macroscopic "slip action". We also observed modes corresponding to the layers sliding past one another, which would likewise aid the mechanical slippage. In case of Form I, the relevant vibrational modes contributing to slipping seen in Figure 6 have frequencies of 230.39, 271.44, 274.81, 286.75 and 290.19 cm^{-1}. The analogous modes in Form III were found to have significantly lower energies of 64.49, 75.31 and 97.25 cm^{-1} (slip along the b axis), and 99.90, 101.51, 113.59-139.31 and 291.73 cm^{-1} (slip along the c axis). We also observed "partial" slip modes in Forms I and III, in which one layer slips while the other displays ring bending, which could also aid in layer separation. The presence of soft phonons which would reinforce the macroscopic slip action suggest that Form III may be mechanically, as well as thermodynamically, unstable compared to the competing phases, which could further explain its rarity.

In contrast, the herringbone packing in Form II does not lend itself to slipping. Despite this, phonon modes similar to the ones observed in the other two forms were visible at 277.69-330.96 cm^{-1} in this polymorph, although this is generally stiffer than in Form I, implying that such motions are less energetically accessible. A list of the relevant modes observed in the three forms, including their frequencies and assignments, can be found in Tables S9-S11.

It is worth noting that one could explain the differences in millability between Forms I/III and II from a simple comparison of the respective crystal structures, and while the conclusions from this analysis are supported by the lattice-dynamics calculations, these are a much more complex means of studying the same phenomenon. On the other hand, the link between the presence of

slip planes and soft phonon modes *is* important in explaining the thermodynamics of the phase equilibria.

Equation of state and mechanical properties

Finally, to investigate further the mechanical properties of the three polymorphs, we also calculated energy/volume (*E/V*) curves (Figure 7), which were then fitted to an equation of state to obtain equilibrium structural parameters, *viz*. the volume, density and bulk modulus (Table 4). The *E/V* curves reproduce the key features of the system observed experimentally and from the lattice-dynamics calculations presented earlier, *viz*. the higher density of Form II compared to the other polymorphs, and the 0 K energetic ordering of Form II < Form I < Form III.

Interestingly, the equation of state suggests that the lattice energies of Forms II and I may come into equilibrium under moderate expansion of Form II. This condition could be met, while simultaneously introducing energy to effect the structural rearrangement, by heating, which provides an additional explanation as to why Form II can be converted to Form I on heating. Indeed, we note that, whereas the thermodynamic equilibrium has been reported to be at around 50-54 ºC (323-327 K), fast conversion is observed only at rather higher temperatures around 160 ºC (433K).(22) Form III has a higher lattice energy over the complete range of volumes studied in this work, reinforcing its thermodynamic instability with respect to the other SMZ polymorphs.

A further piece of information which can be obtained from the *E/V* curves is the common tangent between the minima of Forms I and II, which gives the theoretical pressure at which they would be in equilibrium. We calculated this pressure to be around 500 MPa, which may be accessible by mechanical milling, and which would be consistent with the fact that Form I

converts to Form II on ball milling at RT for an hour.(8) The conversion on milling may also be interpreted in terms of the higher density of Form II. On the other hand, milling will also lead to heating; the fact that the Form II -> Form I transition is not reversible solely through heating suggests that the mechanical stress induced by milling is likely the most important factor, although the heating may well also assist the phase transition.

Finally, we also calculated the complete elastic tensors for optimized structures at the predicted equilibrium volumes using the VASP code.(39, 40) From the elastic tensors, we obtained the corresponding compliance tensors by matrix inversion, and calculated the bulk and shear moduli, universal elastic anisotropies and isotropic Poisson ratios according to the various averaging schemes in Ref. (51). The two sets of tensors and the calculated properties are presented in Tables S12-S18.

The bulk moduli obtained from the elastic tensors are similar to those obtained from the E/V curves, albeit slightly higher. The three compounds all have bulk moduli between 10 and 14 GPa, while the shear moduli are between 1 and 6 GPa. Taking the Voigt-Reuss-Hill average moduli, which fall between the upper and lower bounds predicted by the Voigt and Reuss averages, respectively, the maximum variation in the calculated bulk moduli between the polymorphs is 8.8 %, whereas the variation in the shear moduli is a considerably larger 24.2 %. These differences together give rise to a large difference in the elastic anisotropy, while the differences in Poisson ratio are small, being a maximum of 10.3 %. Unfortunately, we were not able to find experimental measurements of the elastic properties of any of the SMZ polymorphs to compare with our calculations, but the present results may serve as a useful reference for future work.

Discussion

We close with some general comments on the methodology employed in this work. In general, the *ab initio* lattice-dynamics calculations performed on SMZ have shown good agreement with experiment when compared to MIR and Raman spectroscopy, which probe the phonon frequencies, and to the thermal ellipsoids from variable-temperature crystallography, which probe indirectly the atomic displacements which characterize the low-frequency phonon modes.

In terms of thermodynamics, our results suggest that differences in zero-point vibrational energy can be on the same order as differences in lattice energy ($\sim$kJ mol^{-1}), which suggests that including this contribution to the free energy may be important for analyzing polymorph stability even at low temperature, when the effects of phonon occupation on internal energy and entropy are minimal. In the present work, we were able to use the temperature-dependent Helmholtz energy, computed at the room-temperature lattice parameters, to estimate the thermodynamic transition temperature between Forms I and II with reasonable accuracy. This is in spite of the discrepancy between the calculated and measured frequencies of the high-energy phonons, which may be ascribed to the fact that the low-frequency modes are the ones which are significantly populated at low-to-moderate temperature, and so make the most significant contribution to the temperature dependence of the free energy.

However, it is worth noting that, under most experimental conditions, it is the constant-pressure (Gibbs) free energy, rather than the Helmholtz energy, which is relevant. Within the quasi-harmonic approximation,(24, 52) the lattice temperature is assumed to be encoded in the cell volume, and the Gibbs energy at a given temperature is obtained as the Helmholtz energy computed at the corresponding lattice volume. Therefore, it is likely that the good agreement in the transition temperature is due in part to our fixing the unit-cell parameters at the 300 K values,

which in this case happen to be fairly closer to the experimentally-measured transition point. We intend to investigate this further in the future by performing full quasi-harmonic calculations on SMZ.

More generally, given that there are presently few reports of studies attempting to predict transition temperatures using DFT in combination with lattice-dynamics calculations, least of all on systems as complex as molecular crystals, it is difficult to comment on the size of the possible error in the predicted values. In a recent study of $CsSnI_3$,(52) errors in excess of 100 K were observed when using the calculated Helmholtz and Gibbs free energies; however, a complication in this system is that the high-temperature phases are likely to be average structures rather than true energy minima,(52, 53) which we do not believe is the case for SMZ. Even differences of 100+ K amount to subtle differences in energy, which could easily fall within the error associated with e.g. a less-than-optimal choice of DFT functional or a poorly-converged basis set or k-point sampling.

Finally, it is worth noting that we observed qualitative differences in the stability ordering predicted by the three DFT functionals we tested, *viz*. PBE, PBEsol and PBE-D2, with PBE performing particularly poorly for this system. This indicates that in studies such as the present, which aim to probe subtle energetics, it may be important to benchmark several functionals to find the best-performing one for the system under study.

Conclusions

Through the combined experimental and computational study performed in this work, we have obtained a detailed understanding of the polymorphic transformations observed between the

forms of the model API Sulfamerazine, and the relationships between the structures and the industrially-relevant mechanical properties.

In spite of a few caveats, *ab initio* lattice-dynamics calculations have enabled an exploration of the soft phonon modes which give rise to the crystal dynamics visible in the displacement parameters obtained from X-ray diffraction experiments. Thermodynamics calculations successfully reproduced the high-temperature phase transition between Forms II and I, which appears to occur primarily due to the higher vibrational entropy of the latter offsetting differences in internal energy, in particular the lattice energy, at finite temperature. This can be attributed to the layered structure of Form I allowing for softer lattice vibrations than the herringbone packing of Form II. The rarity of Form III can be explained by the fact that at low temperature it has a higher internal energy than either of the competing phases, whereas at high temperature its vibrational entropy is not competitive with that of Form I. We intend to carry out further calculations in the future to investigate the thermal expansion observed in the crystals in more detail, in particular the potential low-temperature anomalies in the expansion of Form II.

From our calculations, we were also able to attribute the easier millability/processability of Form I over Form II to the presence of the slip plane. We identified vibrational modes in Form I which may aid in the slip action, and although some similar modes were observed in Form II, which does not have a slip plane, these were found to occur at higher frequencies, due to the tighter H-bonding network, which indicates that such motions are energetically more difficult in the denser herringbone structure. The slip action in Form III, on the other hand, appears to be supported by very soft lattice phonons, which may lead to this polymorph being mechanically, as well as thermodynamically, unstable.

A comparison of the calculated equations of state of the polymorphs show that the lattice energies of Form II and Form I may come to equilibrium as the Form II lattice is expanded, providing additional evidence for why the conversion from Form II to Form I happens on heating. On the other hand, this analysis suggests that Form I and II would be in equilibrium at a pressure of around 500 MPa, which, combined with the lower density of Form II, suggests why the conversion of Form I to Form II can be effected by ball milling. The microscopic insight obtained from this work may help to improve the processing of SMZ, i.e. milling, compaction, tabletting *etc*., and to direct crystal-engineering approaches to obtain formulations with improved stability and properties, and should also be applicable to other systems such as the widely-studied paracetamol.

In summary, the findings from this study reinforce the results from previous work in the literature, while providing additional insight which may help to rationalize the relative stabilities of the polymorphs in this and in other pharmaceutically-important systems, and also to aid the design of formulations (e.g. cocrystals) with improved stability and properties. Moreover, the computational methodology explored in this work is general, and could be applied to the study of other, perhaps more challenging, systems.
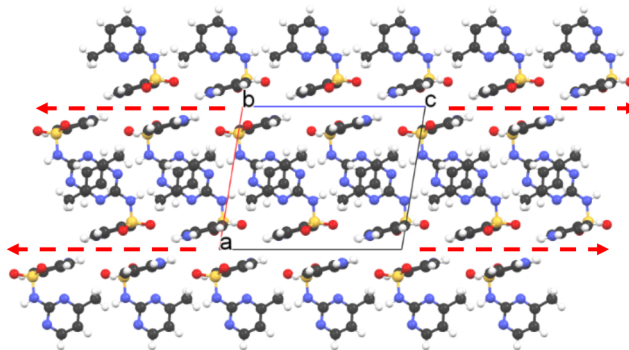
Figures

(a) Form I (*ab* plane)
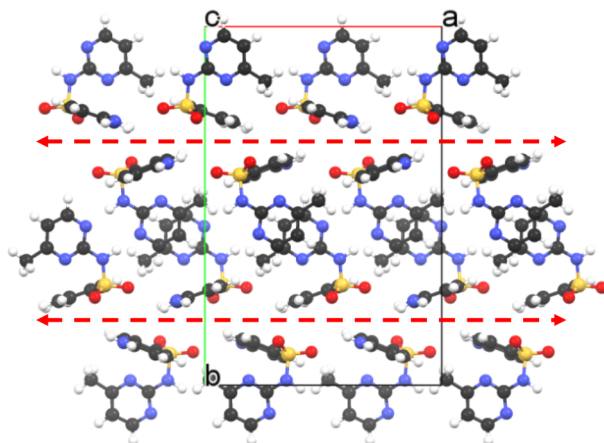
(b) Form II (*bc* plane)
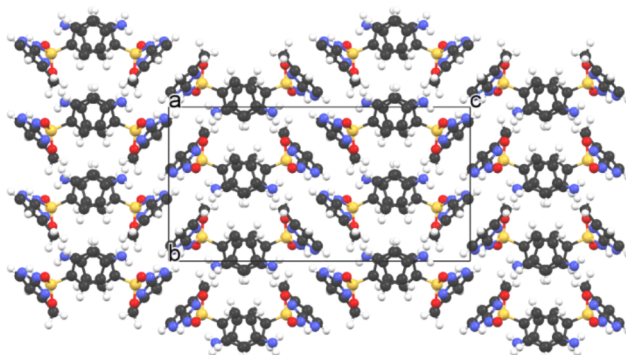
(c) Form III (*ac* plane)

Figure 1. Representative crystal structures of Sulfamerazine Forms I (a), II (b) and III (c), generated from the reported structures(5, 6, 9) using the Mercury software(54). Forms I and III both have slip planes, marked by red dashed arrows, which are visible when viewed along the *c* and *b* axes, respectively, while the herringbone packing in Form II is clearly visible when viewed along the *a* axis.
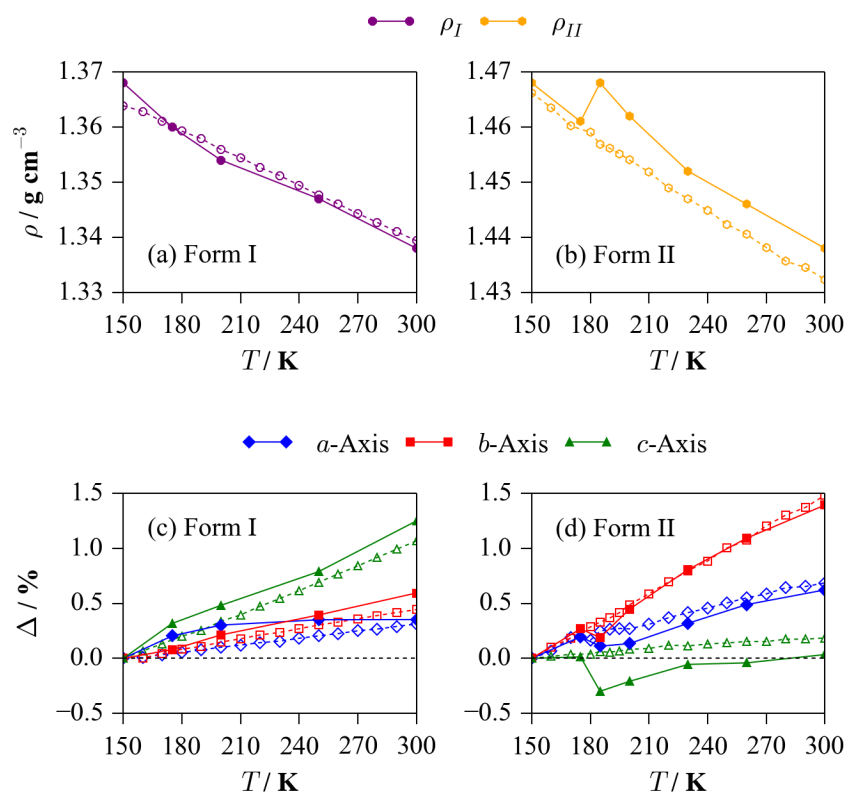
Figure 2. Thermal expansion of Sulfamerazine Forms I and II from single-crystal X-ray diffraction studies. Plots (a) and (b) show the measured density of Form I (a) and II (b) as a function of temperature, while plots (c) and (d) show the corresponding % changes in the lattice constants. On each plot, the open markers/dashed lines represent data collected at the Diamond Light Source, while the filled markers/solid lines show data collected on an in-house diffractometer.
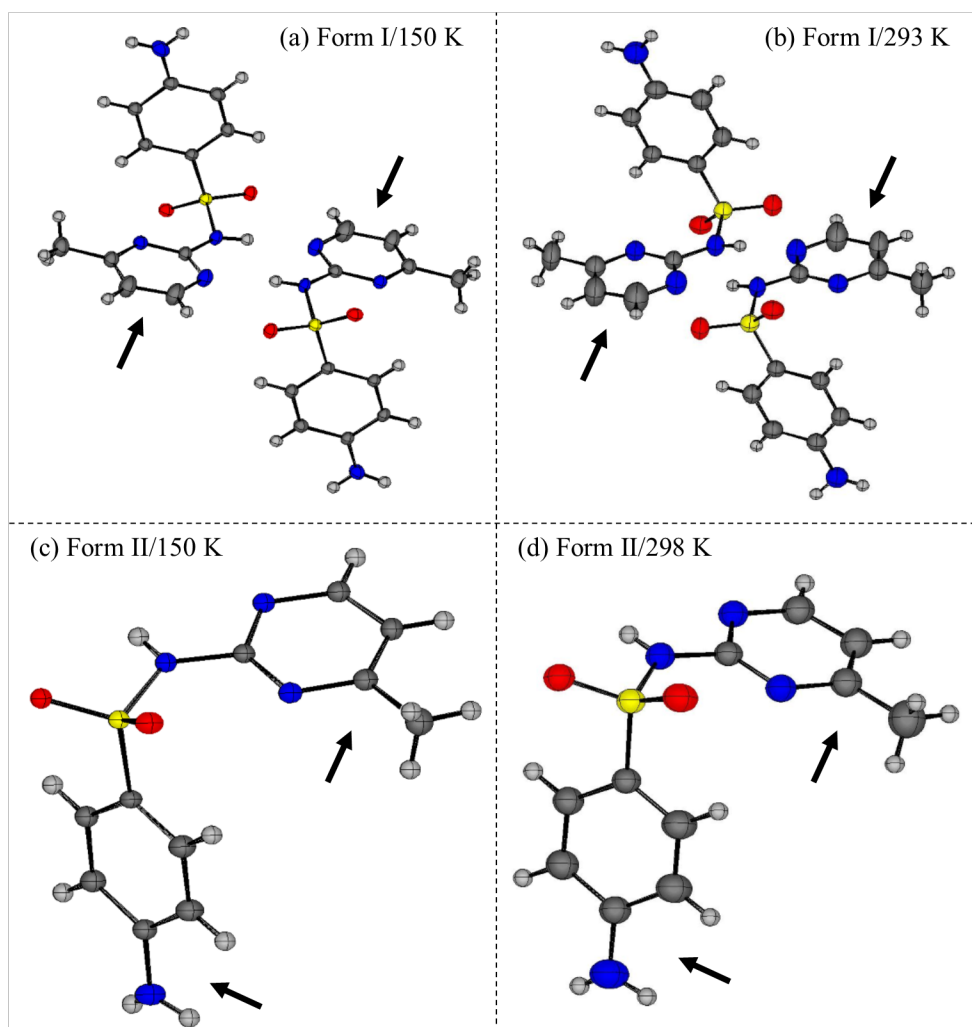
Figure 3. ORTEX plots (30% probability) showing the thermal ellipsoids of Sulfamerazine Forms I (a/b) and II (c/d) at 150 K and room temperature as marked. These structures were obtained from solution and refinement of data collected on an in-house diffractometer (see Experimental). A relative increase in the sizes of the ellipsoids with temperature is observed, as expected, but the pendant rings in both polymorphs exhibit fairly anisotropic ellipsoids (marked by arrows), reflecting soft lattice vibrations corresponding to "rocking" of the rings.
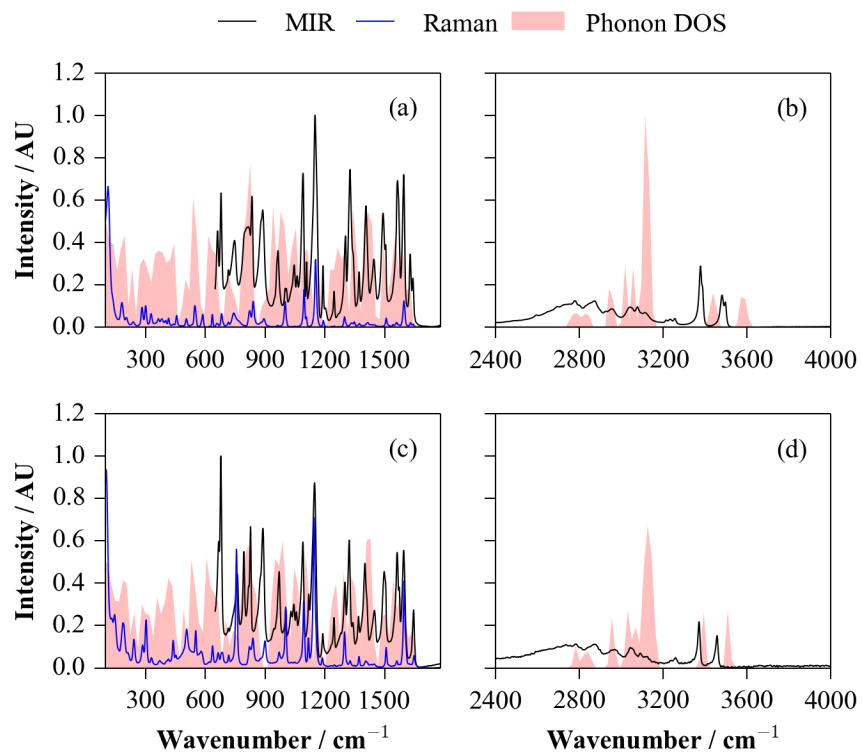
Figure 4. Vibrational spectra of Sulfamerazine Form I (a, b) and Form II (c, d). Plots (a) and (c) compare mid-infrared (MIR) and Raman spectra (785 nm excitation), recorded in the fingerprint region between 100 and 1780 cm^{-1}, to the calculated phonon density of states (DOS). Plots (b) and (d) compare the MIR spectra and phonon DOS between 2400 and 4000 cm^{-1}.
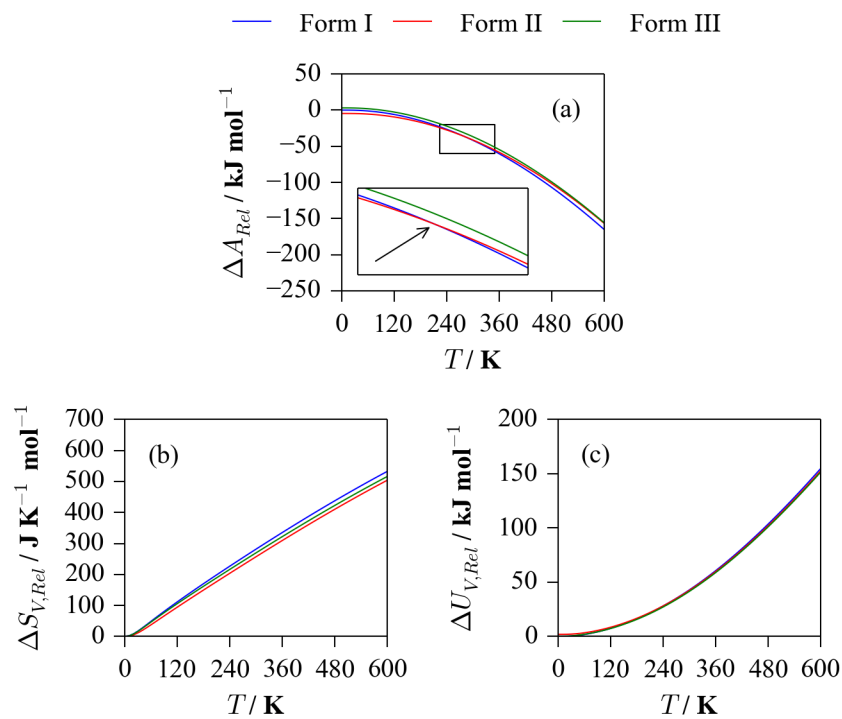
Figure 5. *Ab-initio* thermodynamics of Sulfamerazine Forms I, II and III. The three plots show (a) the calculated constant-volume (Helmholtz) free energy, A, together with the separate contribution from (b) the vibrational entropy, S_V, and (c) the vibrational internal energy, U_V, as a function of temperature, between 0 and 600 K. All four curves are expressed relative to Form I at 0 K.
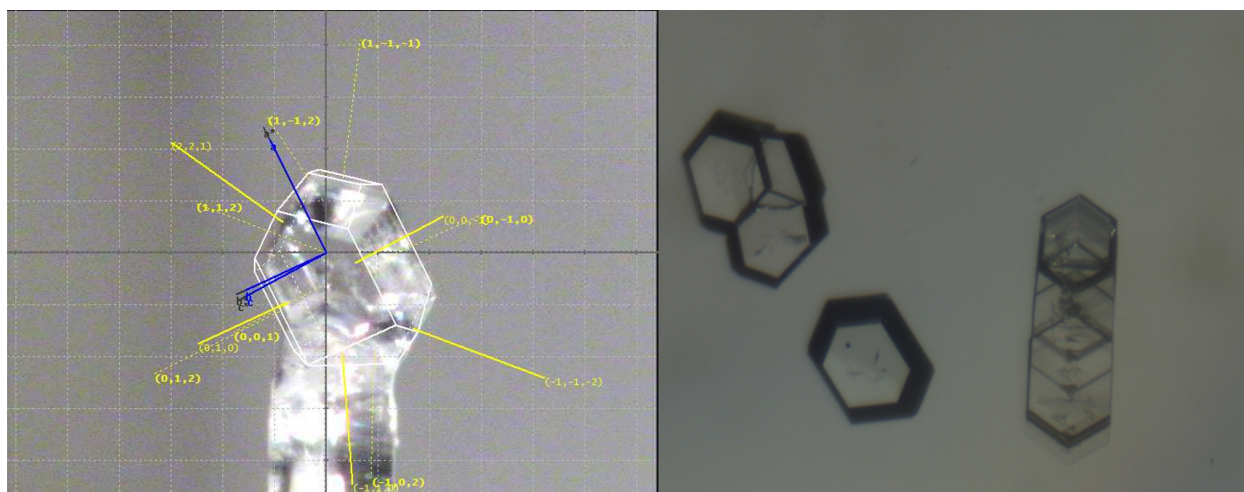
Figure 6. (Left) Indexed faces of a Sulfamerazine Form I crystal. (Right) Layers of Form I formed by slipping along the slip plane normal to the crystallographic *c* axis.
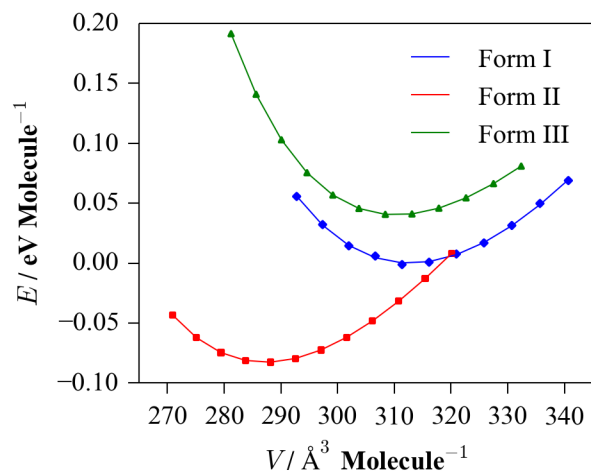
Figure 7. Calculated energy/volume curves for Sulfamerazine Forms I (blue/diamonds), II (red/squares) and III (green/triangles). The markers are the calculated energies, and the solid lines are fits to the Murnaghan equation of state. The equilibrium volumes, densities and bulk moduli obtained from the fits are given in Table 4. The energies are expressed relative to the fitted equilibrium energy of Form I.

Polymorph	a / Å	b / Å	c / Å	α / °	β / °	γ / °
Form I(5)	14.474(2)	21.953(2)	8.2030(10)	90	90	90
Form II(5)	9.145(1)	11.704(1)	22.884(2)	90	90	90
Form III(6)	11.0966(5)	8.3152(5)	13.9640(7)	90	99.327(4)	90

Table 1. Lattice parameters of Sulfamerazine Forms I, II and III collected from the structures reported in Refs. (5) and (6).

Functional	E / Ry Molec^{-1}			ΔE_I / kJ mol^{-1} Molec^{-1}	
	Form I	Form II	Form III	Form II	Form III
Before Mode Following					
PBE	-2389.848	-2389.846	-2389.845	2.62	3.91
PBEsol	-2382.408	-2382.408	-2382.405	-0.49	3.02
PBE-D2	-2389.975	-2389.980	-2389.973	-6.40	2.53
After Mode-Following					
PBE	-2389.849	-2389.846	-2389.845	2.77	4.18
PBEsol	-2382.408	-2382.408	-2382.405	-0.39	3.30
PBE-D2	-2389.975	-2389.980	-2389.973	-6.52	2.80

Table 2. Calculated per-molecule all-electron (PAW) lattice energies of the three polymorphs of Sulfamerazine, computed with three different DFT functionals, before and after the mode-following procedure performed to attempt to remove imaginary phonon modes from the structures (see text). The first three columns give the absolute values in Ry, while the last two give the energies relative to Form I in kJ mol^{-1}.

Functional	U_{ZP} / kJ mol^{-1} Molec^{-1}			$\Delta U_{ZP,I}$ / kJ mol^{-1} Molec^{-1}	
	Form I	Form II	Form III	Form II	Form III
Before Mode Following					
PBE	589.31	591.34	590.10	2.04	0.79
PBEsol	585.73	587.58	586.14	1.85	0.41
PBE-D2	586.63	588.81	587.10	2.18	0.47
After Mode-Following					
PBE-D2	586.90	588.78	487.14	1.88	0.24

Table 3. Calculated per-molecule vibrational zero-point energies of Sulfamerazine Forms I, II and III, obtained from phonon calculations with three different DFT functionals. For PBE-D2, the values after the mode following are also given. As in Table 2, the first three columns give the absolute values (in kJ mol^{-1}), while the last two give the energy differences relative to Form I.

Polymorph	V_0 / Å^3 Molec^{-1}	ϱ_0 / g cm^{-3}	B_0 / GPa
Form I	312.77	1.404	11.44
Form II	287.26	1.528	10.99
Form III	310.39	1.415	11.09

Table 4. Calculated equilibrium volumes, densities and bulk moduli of the three forms of Sulfamerazine, obtained by fitting energy/volume curves to the Murnaghan equation of state (see Figure 7).

Supporting Information. Contains additional figures and tables to support the discussion in the text. Includes DSC curves and the unit-cell parameters recorded in the in-house and synchrotron single-crystal X-ray diffraction measurements, assignments of the various phonon modes which relate to the slip action observed in the different polymorphs, and the calculated elastic/compliance tensors and derived properties. Animations of representative low-frequency lattice vibrations are also supplied. This material is available free of charge via the Internet at http://pubs.acs.org.

Data-Access Statement

The optimized structures and raw data from the phonon calculations are available online free of charge from [URL to be added on acceptance].

Corresponding Author

*Dr Andrea Erxleben (andrea.erxleben@nuigalway.ie), to whom correspondence should be addressed.

Author Contributions

‡These authors contributed equally.

Acknowledgements

Abbreviations

SMZ - Sulfamerazine, DSC - differential scanning calorimetry, TGA - thermogravimetric analysis, MIR - mid-infrared

References

1.   Chieng N, Rades T, Aaltonen J. An overview of recent studies on the analysis of pharmaceutical polymorphs. Journal of Pharmaceutical and Biomedical Analysis. 2011;55(4):618-44.
2.   Lee Y-H, Yang Y-L, Yen W-C, Su W-F, Dai C-A. Solution self-assembly and phase transformations of form II crystals in nanoconfined poly(3-hexyl thiophene) based rod-coil block copolymers. Nanoscale. 2014;6(4):2194-200.
3.   Descamps M, Aumelas A, Desprez S, Willart JF. The amorphous state of pharmaceuticals obtained or transformed by milling: Sub-Tg features and rejuvenation. Journal of Non-Crystalline Solids. 2015;407:72-80.
4.   Venugopalan RPaP. Polymorphism:An Overview. Resonance. 2006:882 - 93.
5.   Caira MR, Mohamed R. Positive identification of 2 orthorhombic polymorphs of sulfamerazine ($C_{11}H_{12}N_4O_2S$), their thermal analyses and structural comparison. Acta Crystallographica Section B-Structural Science. 1992;48:492-8.
6.   Hossain GMG. A new polymorph of sulfamerazine. Acta Crystallographica Section E-Structure Reports Online. 2006;62:O2166-O7.
7.   Aloisio C, de Oliveira AG, Longhi M. Characterization, inclusion mode, phase-solubility and in vitro release studies of inclusion binary complexes with cyclodextrins and meglumine using sulfamerazine as model drug. Drug Development and Industrial Pharmacy. 2014;40(7):919-28.

8.   Macfhionnghaile P, Hu Y, Gniado K, Curran S, McArdle P, Erxleben A. Effects of Ball-Milling and Cryomilling on Sulfamerazine Polymorphs: A Quantitative Study. Journal of Pharmaceutical Sciences. 2014;103(6):1766-78.

9.   Acharya KR, Kuchela KN, Kartha G. Crystal-structure of sulfamerazine. Journal of Crystallographic and Spectroscopic Research. 1982;12(4):369-76.

10.   Cao XP, Sun CQ, Thamann TJ. A study of sulfamerazine single crystals using atomic force microscopy, transmission light microscopy, and Raman spectroscopy. Journal of Pharmaceutical Sciences. 2005;94(9):1881-92.

11.   Cao X, Sun C, Thamann TJ. Surface characterizations of sulfamerazine polymorphs using atomic force microscopy, transmission light microscopy and Raman microspectroscopy. Microscopy and microanalysis : the official journal of Microscopy Society of America, Microbeam Analysis Society, Microscopical Society of Canada. 2005;11 Suppl 2:378-9.

12.   Davis T, Johnson M, Billinge SJL. Toward Phase Quantification at the Nanoscale Using the Total Scattering Pair Distribution Function (TSPDF) Method: Recrystallization of Cryomilled Sulfamerazine. Crystal Growth & Design. 2013;13(10):4239-44.

13.   Delgado DR, Martinez F. Solubility and solution thermodynamics of sulfamerazine and sulfamethazine in some ethanol plus water mixtures. Fluid Phase Equilibria. 2013;360:88-96.

14.   Gong Y, Collman BM, Mehrens SM, Lu E, Miller JM, Blackburn A, et al. Stable-form screening: Overcoming trace impurities that inhibit solution-mediated phase transformation to the stable polymorph of sulfamerazine. Journal of Pharmaceutical Sciences. 2008;97(6):2130-44.

15.   Gu CH, Chatterjee K, Young V, Grant DJW. Stabilization of a metastable polymorph of sulfamerazine by structurally related additives. Journal of Crystal Growth. 2002;235(1-4):471-81.

16.   Kurotani M, Hirasawa I. Effect of ultrasonic irradiation on the selective polymorph control in sulfamerazine. Chemical Engineering Research & Design. 2010;88(9A):1272-8.

17.   Lee S, Choi A, Kim W-S, Myerson AS. Phase Transformation of Sulfamerazine Using a Taylor Vortex. Crystal Growth & Design. 2011;11(11):5019-29.

18.   Lee M-J, Seo D-Y, Wang I-C, Chun N-H, Lee H-E, Jeong M-Y, et al. Quantitative in-line monitoring of solvent-mediated polymorphic transformation of sulfamerazine by near-infrared spectroscopy. Journal of Pharmaceutical Sciences. 2012;101(4):1578-86.

19.   Lou H, Liu M, Qu W, Johnson J, Brunson E, Almoazen H. The influence of sodium salts (iodide, chloride and sulfate) on the formation efficiency of sulfamerazine nanocrystals. Pharmaceutical Development and Technology. 2014;19(5):548-55.

20.   Roy S, Alexander KS, Riga AT, Chatterjee K. Characterization of physical mixtures and directly compressed tablets of sulfamerazine polymorphs: Implications on in vitro release characteristics. Journal of Pharmaceutical Sciences. 2003;92(4):747-59.

21.   Sun CQ, Grant DJW. Influence of crystal structure on the tableting properties of sulfamerazine polymorphs. Pharmaceutical Research. 2001;18(3):274-80.

22.   Zhang GGZ, Gu CH, Zell MT, Burkhardt RT, Munson EJ, Grant DJW. Crystallization and transitions of sulfamerazine polymorphs. Journal of Pharmaceutical Sciences. 2002;91(4):1089-100.

23.   Sun CC, Kiang YH. On the identification of slip planes in organic crystals based on attachment energy calculation. Journal of Pharmaceutical Sciences. 2008;97(8):3456-61.

24.   Skelton JM, Parker SC, Togo A, Tanaka I, Walsh A. Thermal physics of the lead chalcogenides PbS, PbSe, and PbTe from first principles. Physical Review B. 2014;89(20):205203.

25.   Sheldrick GM. SHELXT. Acta Crystallogr A. 2015;71:3-8.
26.   G. M. Sheldrick. SHELXL Acta Crystallogr C. 2015;71: 3-8.
27.   Ardle PM. PC Windows version. JApplCryst. 1995;28:65.
28.   Dove MT. Introduction to Lattice Dynamics. Cambridge, UK: Cambridge University Press; 1993.
29.   Parlinski K, Li ZQ, Kawazoe Y. First-principles determination of the soft mode in cubic ZrO_2. Physical Review Letters. 1997;78(21):4063-6.
30.   Giannozzi P, Baroni S, Bonini N, Calandra M, Car R, Cavazzoni C, et al. QUANTUM ESPRESSO: a modular and open-source software project for quantum simulations of materials. Journal of Physics-Condensed Matter. 2009;21(39).
31.   Perdew JP, Burke K, Ernzerhof M. Generalized gradient approximation made simple. Physical Review Letters. 1996;77(18):3865-8.
32.   Perdew JP, Ruzsinszky A, Csonka GI, Vydrov OA, Scuseria GE, Constantin LA, et al. Restoring the density-gradient expansion for exchange in solids and surfaces. Physical Review Letters. 2008;100(13).
33.   Constantin LA, Pitarke JM, Dobson JF, Garcia-Lekue A, Perdew JP. High-level correlated approach to the jellium surface energy, without uniform-gas input. Physical Review Letters. 2008;100(3).
34.   Grimme S. Semiempirical GGA-type density functional constructed with a long-range dispersion correction. Journal of Computational Chemistry. 2006;27(15):1787-99.
35.   Blochl PE. Projector augmented-wave method. Physical Review B. 1994;50(24):17953-79.
36.   Monkhorst HJ, Pack JD. Special points for brillouin-zone integrations. Physical Review B. 1976;13(12):5188-92.
37.   Togo A, Oba F, Tanaka I. First-principles calculations of the ferroelastic transition between rutile-type $CaCl_2$ and SiO_2 at high pressures. Physical Review B. 2008;78(13):134106.
38.   Murnaghan FD. The Compressibility of Media Under Extreme Pressures. Proceedings of the National Academy of Sciences of the United States of America. 1944;30:244-7.
39.   Kresse G, Hafner J. Abinitio molecular-dynamics for liquid-metals. Physical Review B. 1993;47(1).
40.   Le Page Y, Saxe P. Symmetry-general least-squares extraction of elastic data for strained materials from \textit{ab initio} calculations of stress. Physical Review B. 2002;65(10):104104.
41.   Kresse G, Joubert D. From ultrasoft pseudopotentials to the projector augmented-wave method. Physical Review B. 1999;59(3).
42.   Wright JD. Molecular motion in crystal; Molecular Crystals. Great Britain1987.
43.   Deringer VL, Stoffel RP, Togo A, Eck B, Meven M, Dronskowski R. Ab initio ORTEP drawings: a case study of N-based molecular crystals with different chemical nature. Crystengcomm. 2014;16(47):10907-15.
44.   Filippi C, Singh DJ, Umrigar CJ. All-Electron Local-Density and Generalized-Gradient Calculations of the Structural-Properties of Semiconductors. Physical Review B. 1994;50(20):14947-51.
45.   Khein A, Singh DJ, Umrigar CJ. All-Electron Study of Gradient Corrections to the Local-Density Functional in Metallic Systems. Physical Review B. 1995;51(7):4105-9.
46.   Haas P, Tran F, Blaha P. Calculation of the lattice constant of solids with semilocal functionals. Physical Review B. 2009;79(8).

47.   Lee IH, Martin RM. Applications of the generalized-gradient approximation to atoms, clusters, and solids. Physical Review B. 1997;56(12):7197-205.

48.   Li Y, Chow PS, Tan RBH. Quantification of polymorphic impurity in an enantiotropic polymorph system using differential scanning calorimetry, X-ray powder diffraction and Raman spectroscopy. International Journal of Pharmaceutics. 2011;415(1-2):110-8.

49.   Chang C-F, Okajima H, Hamaguchi H-o, Shigeto S. Imaging molecular crystal polymorphs and their polycrystalline microstructures in situ by ultralow-frequency Raman spectroscopy. Chemical Communications. 2014;50(85):12973-6.

50.   Chang C-F, Wang S-C, Shigeto S. In Situ Ultralow-Frequency Raman Tracking of the Polymorphic Transformation of Crystalline 1,1 '-Binaphthyl. Journal of Physical Chemistry C. 2014;118(5):2702-9.

51.   de Jong M, Chen W, Angsten T, Jain A, Notestine R, Gamst A, et al. Charting the complete elastic properties of inorganic crystalline compounds. Scientific Data. 2015;2:150009.

52.   da Silva EL, Skelton JM, Parker SC, Walsh A. Phase stability and transformations in the halide perovskite ${\mathrm{CsSnI}}_{3}$. Physical Review B. 2015;91(14):144107.

53.   Huang L-y, Lambrecht WRL. Lattice dynamics in perovskite halides CsSnX with X = I, Br, Cl. Physical Review B. 2014;90(19):195201.

54.   F. Macrae, I. J. Bruno, J. A. Chisholm, P. R. Edgington, P. McCabe, E. Pidcock, et al. Mercury CSD 2.0 - New Features for the Visualization and Investigation of Crystal Structures C. . J Appl Cryst. 2008;41: 466-70